Knowledge E
Engaging minds

Conference Paper

The ALICE CPV detector

S Evdokimov, V Izucheev, Yu Kharlov, E Kondratyuk, S Sadovsky, and A Shangaraev for the ALICE collaboration

NRC "Kurchatov Institute" – IHEP, Protvino, Russia

Abstract

The Charged-Particle Veto (CPV) detector of ALICE at the LHC is presented. Physics motivation for the detector, its construction and operation in physics runs are shortly discussed. Readout electronics and data taking conditions are described. Special attention is focused on CPV automation via the detector control system. Different states of the detector and protection algorithms implemented into the control system are described.

Corresponding Author:
E Kondratyuk
evgeny.kondratyuk@cern.ch

Received: 25 December 2017
Accepted: 2 February 2018
Published: 9 April 2018

Publishing services provided by Knowledge E

Selection and Peer-review under the responsibility of the ICPPA Conference Committee.

1. Introduction

The Charged-Particle Veto detector (CPV) is a multi-wire proportional chamber with cathode pad readout placed on the top of one Photon spectrometer (PHOS) module [1] of ALICE [2] to suppress charged-particle background of the direct photon sample detected in PHOS. Its main purpose is to improve neutral-cluster identification in PHOS.

One of the tasks of ALICE is to study photons emitted directly from pp or Pb–Pb collision, so-called "direct photons". ALICE is equipped with a high-precision photon spectrometer PHOS, consisting of four modules with a total of 12544 $PbWO_4$ crystals each one of size 2.2x2.2x18 cm^3. For measuring the photon spectra it is crucial to have a good photon identification, especially in Pb–Pb-collisions. The signal of thermal photon radiation from hot QCD matter produced in AA collisions is expected to be observed in the range $1 < p_T < 4$ GeV/c as a small excess over the photon spectrum from hadron decays. Methods of photon identification were discussed in the ALICE Technical Design Report [1] and in the Physics Performance Report [3] and include 3 methods. The first uses the shower shape of PHOS clusters to discriminate electromagnetic and hadronic showers. The second one uses cluster timing in PHOS to discriminate fast particles (photons, electrons) from slow particles (heavier hadrons). The third method requires the CPV detector [4] to match PHOS clusters and charged-particle tracks. This allows one to discriminate neutral clusters in PHOS (photons) from the charged clusters (electrons, charged hadrons).

2. Construction

2.1. General description

CPV is a proportional chamber with cathode pad readout. Though there are only anode co-directional wires and cathode plane, it is possible to measure 2-D coordinates using the induced charge distribution on the pads [5]. Charged tracks pass through the CPV ionizing the gas mixture. Slow-moving ions induce charges on pads of the segmented cathode, which are detected by the readout electronics. The ion cloud projects the charge on several pads of the cathode which compose a cluster. We consider clusters of 4 or more pads, from which cluster coordinates in CPV are reconstructed. The cluster coordinates (x,z) in CPV are calculated as the first moments of the charge distribution weighted with the logarithm of the pad amplitude [6], so it is possible to find hit coordinates with accuracy much better than the pad size. CPV is able to measure charged track hits in (x,y) plane with an accuracy of 0.7-1 mm.

CPV is positioned at 12 cm above the front crystal surface in the PHOS module, thus cluster matching in PHOS and CPV is used for photon identification. Matching of a PHOS and a CPV cluster means that the PHOS cluster was produced by a charged particle. PHOS clusters without matched CPV clusters correspond to neutral particles. The main characteristics of the CPV detector are presented in Tab. 1. General view of the CPV module is presented in Fig. 1.

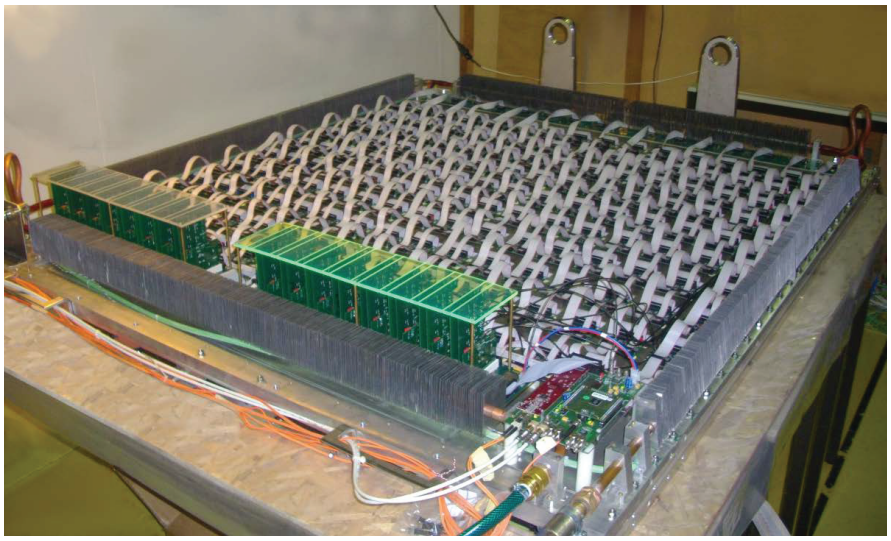

Figure 1: A general view of the CPV detector without the safety cover in the laboratory. One can see the readout electronics at the CPV surface: columns of 3Gassiplex cards connected with flat cables, Dilogic cards on top of segment boards under the green plexiglass and the RCB card in the right bottom side.

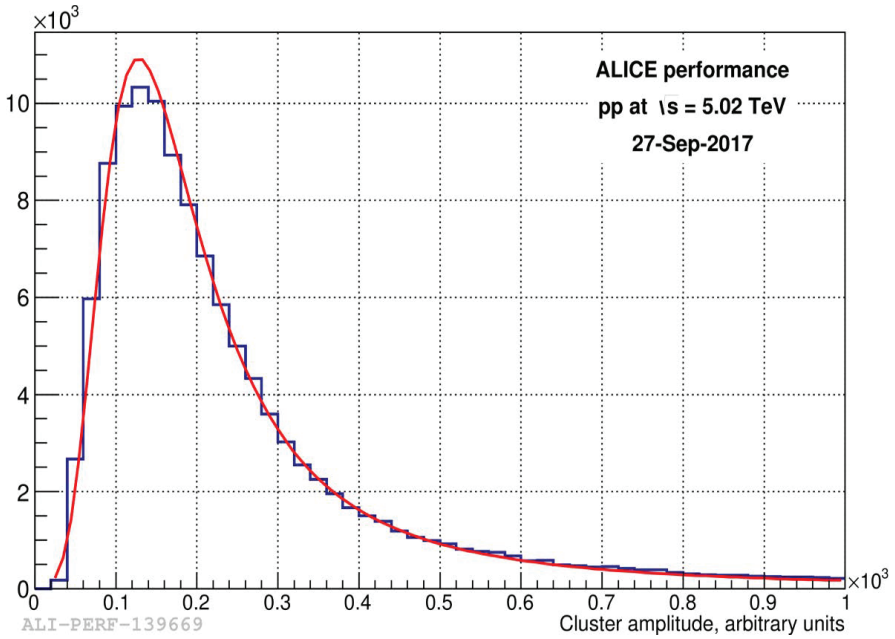

Figure 2: Amplitude spectrum of CPV clusters matched with charged tracks reconstructed in the central-tracking system in pp collisions at 5.02 TeV. The red continuous line is a fit to a Landau function.

Table 1: Main characteristics of the CPV detector

Sensitive volume size:	140 x 123 x 1.4 cm^3
Wire pitch	5.6 mm
Wire diameter	28 μm
Number of sensitive wires	258
Wire tension	100 g
Anode-cathode spacing	7 mm
Pad size	21 x 10 mm^2
Transverse segmentation	128x60 pads
Number of channels with charge-sensitive amplifiers	7680
Gas mixture	Ar(80%)+CO_2 (20%)
Nominal anode HV	2.2 kV (+)
Material budget	5% X_0
Designed coordinate resolution	≈1 mm

2.2. Readout electronics

The key component of the CPV electronics are 160 3Gassiplex cards assembled in a matrix with 16 columns and 10 rows. Each 3Gassiplex card includes 48 channels of charge-sensitive amplifiers with multiplexed readout [7]. It is connected via a coaxial cable to the relevant Dilogic card [8]. One Dilogic card has 5 ADC (12 bit) channels, so it digitizes signals from five 3Gassiplex cards simultaneously, i.e. from 5x48 channels. Two Dilogic cards are used for signal digitization from 3Gassiplex cards assembled in

one column. One Column Controller (CC) controls the process of reading these 3Gassiplex cards and signal digitization from two Dilogic cards. The signal processing from the full CPV module is controlled thus by 16 CC, which together with their Dilogic cards are installed on two Segment (mother) boards. Each Segment provides sequantial sparse readout of 8 CC and transfers data to the Readout Control Board (RCB-card). The latter has optical interfaces to the DAQ (DDL) and Trigger (TTC) systems, for further details see [1] and [9]. CPV readout time in Run 2 is about 200 μs for low-multiplicity events and $\approx$1800 μs for a fully occupied module. The data readout rate was 5 kHz in pp and 4 kHz in Pb–Pb collisions.

3. Detector control system

3.1. General concept

The detector control system (DCS) is a tool to control the experiment all the time. In a large experiment like ALICE it is built as a tree-like hierarchical system, where each structural level represents a logical element or a physical part of the hardware. The states of upper levels or nodes depend on lower-level ones. CPV is integrated in this system and represents one of such branches. During the ALICE operation the DCS commands are issued on the top node and propagated to the lower ones. Statuses of the systems are read vice versa: they are summarized on the lower levels into a single state on the top node. The main task of the DCS is to switch correctly the detector states using the finite state machine (FSM) paradigm. Also it is crucial to ensure safe operation of the detectors during the physics runs using different automatic checks and procedures and fix all failures without stopping the physics run, if possible. The CPV DCS controls the following hardware: 1 low-voltage (LV) 6-channel power supply Wiener Marathon PL512 and 1 high-voltage (HV) 4-channel power supply Iseg ECH238, 9 temperature sensors inside the CPV module measured by the embedded local monitored board (ELMB) [10], a water valve with sensor for cooling, and gas-condition monitoring tools. The latter is provided by the ALICE gas service. Software is CERN-wide standard: Siemens WinCC system of slow control [11]+JCOP framework, developed by the CERN team [12]. The CPV DCS is hosted on a single computer. All the finite states of the detector (Tab. 2) are set up according to the central DCS team's requirements. There are a lot of checks happening during the transition between the main states to ensure the correct conditions at all times. This can slow a bit all the procedures because devices cannot react instantly to the changes, but CPV can be switched on relatively fast, it takes less than a minute to go from the state "off" to the state "ready".

Table 2: The possible FSM states of the detector.

State	Safety matrix	LV/HV	Run type	When
Ready	not_safe	LV on, HV=2280V	Physics	stable beam, cosmic
Stby_configured	safe	LV on, HV=1000V	Technical, pedestal	normal injection, beam tuning
Standby	supersafe	LV on, HV off	Technical	harmful injection
Off	supersafe	LV off, HV off	None	L3 magnet ramp

3.2. Safety

CPV as a wire chamber can be easily damaged by the incorrect run conditions. To prevent this, the CPV DCS has a number of safety scripts (software interlocks), which monitor the state of the detector. The most important is the LV-HV interlock: low voltage powers up readout electronics, high voltage powers up wires, but HV without LV can burn the electronics, so we need to prevent this. Such situation happened several times for the past years because of global power blackouts. The temperature interlock is also important. If electronics inside the CPV are overheated or any of power supplies overheat, it will be switched off. Water and gas interlocks check concentration, flow and pressure in the systems, to ensure that parameters are in pre-set limits. There is also an interlock to recover CPV from high-voltage trips. A HV trip is a discharge inside the gas volume, between wire and pads. It can be detected as a high current in the HV power supply or with the data quality plots online. During the trip the global run is safely paused for about 15 seconds while the corresponding channel is switching off. Notifications about hardware failures and software interlocks are distributed in this case via the ALICE alarm panel and via e-mails.

4. Performance

The CPV works stable for collision rates up to 160 kHz. HV trips were observed in runs with high particle flux: Pb–Pb, high-luminosity p–Pb and pp collisions. We studied the dependence of amplification and stablility on the gas mixture and the high-voltage setting. Amplification increases with higher HV and decreases with higher percentage of CO_2. There is no direct dependence between probability of HV trip and other parameters, but it seems that it decreases with increasing of CO_2 percentage. After the high luminosity pp collisions with the interaction rate of 700 kHz we tuned the gas mixture to 80% Ar + 20% CO_2 and the HV to 2280 volts.

Calibration is done permanently during the data-taking. A dedicated online detector algorithm is supposed to gather amplitude histograms for every CPV channel (1 channel = 1 pad) to further use them to define gain-calibration coefficients. These histograms

are fit to a Landau function when statistics is sufficient. The Landau-function parameter "Mean" determines the calibration coefficient as follows: calibration = 200 / Mean (in arbitrary units).

The bad-channel map (BCM) is also permanently updated during physics runs. Channels with occupancy more then 10 times larger than the mean occupancy are called noisy and added to the BCM, the mean occupancy is then recalculated. This procedure continues until no noisy channels are found. When the procedure finishes, it begins to gather new statistics. Dead channels with value equal zero are also included in the BCM by processing pedestal data.

We have analyzed pp collisions at 5.02 TeV to estimate the quality of the CPV data. Reconstructed tracks from the inner tracking system were propagated to the CPV surface. We chose events where both track and CPV cluster were found. A CPV cluster has to have 4 or more pads in it. The induced charge (Fig. 2) is defined by the ionization energy loss of charged particles passing through the CPV which is well described by a Landau distribution (red continuous curve). For these events, the matching distance along the z axis between the CPV cluster and the projection of the global track to the CPV surface was calculated (Fig. 3). The main peak in the distribution corresponds to clusters produced by reconstructed charged tracks, while the background are clusters uncorrelated with global tracks. The peak position is displaced 3.3 cm which can be explained by the CPV misalignment with respect to the central-tracking system.

We also calculated the distance along the z axis between the CPV cluster and PHOS clusters at the same energy (Fig. 4). The main peak in the distribution corresponds to PHOS clusters produced by charged tracks which were also detected as CPV clusters, while the background is due to PHOS and CPV uncorrelated clusters. A photon is identified as cluster outside the width of this main peak or as cluster without the relative track.

5. Conclusion and plans

One module of the Charged-Particle Veto for the PHOS spectrometer was produced and installed in the ALICE pit. It was fully integrated into the ALICE DCS and ECS. Its performance was tested in the laboratory and during data taking. Clusters in CPV, PHOS and TPC tracks are correlated. We are looking forward to the first direct photons measurements in Pb–Pb collisions during Run 2 at the LHC as CPV provides such abilities to reject charged-particle clusters from PHOS. We plan to produce and install two more modules during LHC LS2 in 2018-2020. Front-end electronics will be modified for the purposes of HL-LHC, so CPV will be suitable for the high collision rates as well.

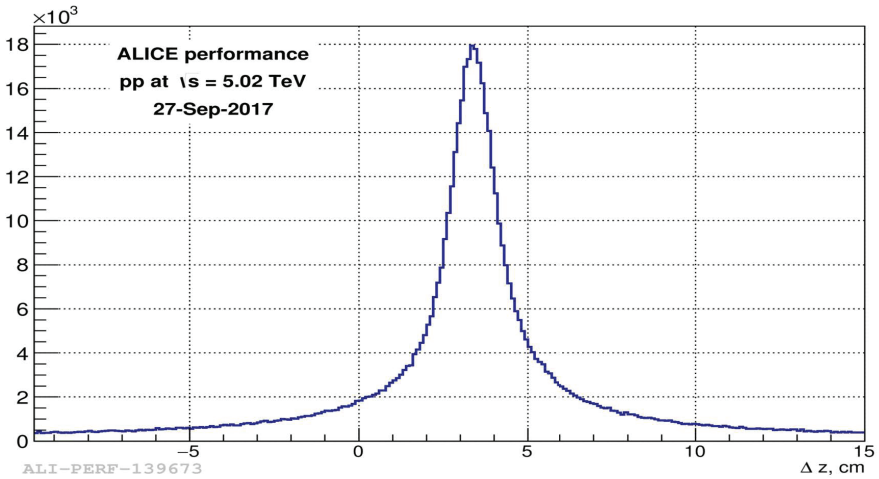

Figure 3: Matching distance along the z axis between the CPV cluster and projection of the global track to the CPV surface. Analysis of pp collisions at 5.02 TeV.

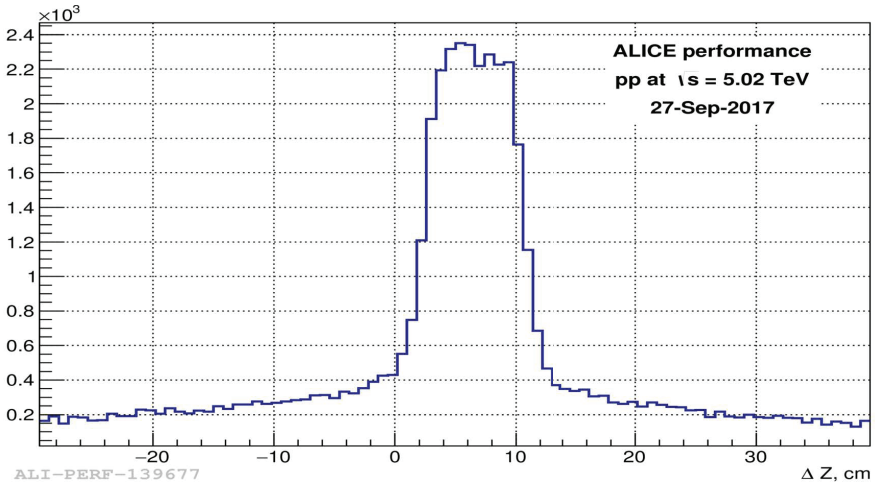

Figure 4: Matching distance along the z axis between the CPV cluster and PHOS clusters at energy $1 < E < 2$ GeV in pp collisions at 5.02 TeV.

Acknowledgments

CPV performance research was supported by the Russian Science Foundation grant 17-72-20234.

References

[1] G. Dellacasa *et al.* [ALICE Collaboration], "ALICE technical design report of the photon spectrometer (PHOS)," CERN-LHCC-99-04.

[2] K. Aamodt *et al.* [ALICE Collaboration], "The ALICE experiment at the CERN LHC," JINST **3** (2008) S08002. doi:10.1088/1748-0221/3/08/S08002

[3] B. Alessandro *et al.* [ALICE Collaboration], "ALICE: Physics performance report, volume II," J. Phys. G **32** (2006) 1295. doi:10.1088/0954-3899/32/10/001

[4] A. M. Blick *et al.*, "A charged-particle detector based on proportional tubes with a segmented cathode and cathode readout," Instrum. Exp. Tech. **44** (2001) 339 [Prib. Tekh. Eksp. **2001** (2001) no.3, 63]. doi:10.1023/A:1017524523571

[5] M. Y. Bogolyubsky *et al.* [ALICE Collaboration], "Charged Particle Veto Detector with Open Geometry for the PHOS Spectrometer," ALICE-INT-2000-21, CERN-ALICE-INT-2000-21.

[6] M. Y. Bogolyubsky *et al.* [ALICE Collaboration], "Charged Particle Veto Detector for the PHOS Spectrometer," ALICE-INT-1999-08, CERN-ALICE-INT-1999-08.

[7] J. C. Santiard *et al.* [ALICE Collaboration], "The GASSIPLEX0.7-2 integrated front-end analog processor for the HMPID and the dimuon spectrometer of ALICE," CERN-ALICE-PUB-2001-49, CERN-ALI-2001-049.

[8] J. C. Santiard, "The ALICE HMPID on-detector front-end and readout electronics," Nucl. Instrum. Meth. A **518** (2004) 498. doi:10.1016/j.nima.2003.11.068

[9] G. Aglieri Rinella *et al.* [ALICE Collaboration], "The level 0 pixel trigger system for the ALICE experiment," JINST **2** (2007) P01007. doi:10.1088/1748-0221/2/01/P01007

[10] B. Hallgren, H. Boterenbrood, H. J. Burckhart and H. Kvedalen, "The embedded local monitor board (ELMB) in the LHC front-end I/O control system,"

[11] SCADA System Siemens WinCC `http://w3.siemens.com/mcms/automation/`

[12] JCOP Framework `http://jcop.web.cern.ch/jcop-framework`